Pharmacologic properties of AG-012986, a pan-cyclin-dependent kinase inhibitor with antitumor efficacy

Cathy Zhang,[1] Karen Lundgren,[1] Zhengming Yan,[1] Maria E. Arango,[1] Sharon Price,[1] Andrea Huber,[1] Joseph Higgins,[1] Gabriel Troche,[1] Judith Skaptason,[2] Tatiana Koudriakova,[2] Jim Nonomiya,[4] Michelle Yang,[5] Patrick O'Connor,[1] Steve Bender,[1] Gerrit Los,[1] Cristina Lewis,[4] and Bart Jessen[3]

Departments of [1]Cancer Biology, [2]Pharmacokinetics, Dynamics and Metabolism, [3]Drug Safety Research and Development, [4]Biochemical Pharmacology, and [5]Medicinal Chemistry, Pfizer Global Research and Development, La Jolla, California

Abstract

AG-012986 is a multitargeted cyclin-dependent kinase (CDK) inhibitor active against CDK1, CDK2, CDK4/6, CDK5, and CDK9, with selectivity over a diverse panel of non-CDK kinases. Here, we report the potent antitumor efficacies of AG-012986 against multiple tumor lines *in vitro* and *in vivo*. AG-012986 showed antiproliferative activities *in vitro* with IC_{50}s of <100 nmol/L in 14 of 18 tumor cell lines. *In vivo*, significant antitumor efficacy induced by AG-012986 was seen (tumor growth inhibition, >83.1%) in 10 of 11 human xenograft tumor models when administered at or near the maximum tolerated dose for 8 or 12 days. AG-012986 caused dose-dependent hypophosphorylation at Ser^{795} of the retinoblastoma protein, cell cycle arrest, and apoptosis *in vitro*. Colony-forming assays indicated that the potency of AG-012986 substantially decreased with treatment time of <24 h. *In vivo*, AG-012986 also showed dose-dependent retinoblastoma Ser^{795} hypophosphorylation, cell cycle arrest, decreased Ki-67 tumor staining, and apoptosis in conjunction with antitumor activity. Studies comparing i.p. bolus with s.c. implanted minipump dosing regimens revealed that *in vivo* efficacy correlated with the duration of minimally effective plasma levels rather than maximal drug plasma levels. Dosing optimization of AG-012986 provided guidance for selecting a treatment schedule to achieve the best antitumor efficacy while minimizing the risk of adverse side effects. [Mol Cancer Ther 2008;7(4):818–28]

Introduction

Cyclin-dependent kinases (CDK) and their regulatory cyclin partners play critical roles in cell cycle control and the regulation of cell transcription. Progression through the different stages of cell cycle is governed by the activities of the CDK1, CDK2, CDK4, CDK6, and possibly CDK3. CDK4/cyclin D, CDK6/cyclin D, and CDK2/cyclin E phosphorylate the retinoblastoma (Rb) protein at multiple sites, which results in activation of the E2F family of transcription factors and serves as a trigger for cells to advance beyond the G_1 checkpoint into S phase (1–3). During S phase, CDK2/cyclin A phosphorylates several proteins, including E2F, to regulate progression through S phase. In fact, it is the phosphorylation and inactivation of the E2F/DP1 transcription factor by CDK2 that is partially responsible for orchestrating an orderly exit from S phase, and interference with this process can lead to apoptosis (4). CDK1/cyclin B functions during G_2-M to initiate mitosis, and it also phosphorylates members of the antiapoptotic protein family, including survivin and Mcl-1. Inhibition of this phosphorylation can result in apoptosis and anticancer activity *in vivo* (5). CDK7, CDK8, CDK9, and CDK11 are involved with regulation of transcription, and CDK7 also phosphorylates and directly regulates other CDKs. The inhibition of CDK9 has been reported to cause down-regulation of Mcl-1 protein through RNA polymerase II–dependent transcription, resulting in tumor cell apoptosis (6, 7).

Several CDK pathways, particularly those involved in cell cycle control, are deregulated and activated in most human cancers in a variety of ways and this activation contributes to tumorigenesis. Therefore, CDKs have been extensively pursued as cancer pharmacology targets, but many of the first-generation CDK inhibitors have suffered from poor potency, selectivity, or efficacy (8). Flavopiridol was the first CDK inhibitor to advance to the clinic. It is a broad-spectrum moderately potent CDK inhibitor and inhibits CDK1, CDK2, CDK4, CDK6, CDK7, and CDK9 with IC_{50}s in the 0.1 to 0.4 μmol/L range (9). *R*-roscovitine (seliciclib, currently in phase II trials), a purine-based CDK inhibitor, appears to be more selective toward CDK1, CDK2, CDK7, and CDK9 than CDK4, CDK6, and CDK8 (10), although the lack of potency of this compound makes broad-spectrum selectivity difficult to assess. The efficacies of flavopiridol (9) and seliciclib (11) in solid tumor models have been shown to correlate with the inhibition of cell cycle progression through apparent cytostatic growth

Received 6/28/07; revised 12/6/07; accepted 2/8/08.

The costs of publication of this article were defrayed in part by the payment of page charges. This article must therefore be hereby marked *advertisement* in accordance with 18 U.S.C. Section 1734 solely to indicate this fact.

Note: All authors are present or former employees of Pfizer. The current address of former Pfizer employees is available upon request.

Requests for reprints: Cathy Zhang, Department of Cancer Biology, Pfizer Global Research and Development, 10724 Science Center Road, San Diego, CA 92121. Phone: 858-622-3125.
E-mail: cathy.zhang@pfizer.com

doi:10.1158/1535-7163.MCT-07-0440

arrest. Both of these drugs also inhibit CDK9, and at least part of the mechanism for the induction of apoptosis in hematopoietic tumor cell lines has been attributed to the inhibition of CDK9-mediated cellular transcription (7, 12). Indolinone-based CDK inhibitors (e.g., SU9516) follow a similar inhibitory pattern as purine-based inhibitors, with increased potency (6). Greater potency and selectivity toward CDK2 has recently been achieved with compounds such as PHA533533 and BMS-387032 (8). PD332991 is unique among the CDK inhibitors for its potency and high selectivity for CDK4/6 over other CDKs and kinases (13), and this compound is currently in phase I/II clinical trials.

Our understanding of the complexity of the roles of the CDKs has continued to grow in recent years. Published data have suggested that cells can recover from targeted inhibition of a single CDK likely by compensatory activity from other CDKs (14, 15). Therefore, a multitargeted or pan-CDK inhibitor may be preferred for more robust antitumor efficacy. Based on this principle, the multitargeted CDK inhibitor, AG-012986, was designed and assessed for the antiproliferative activity in tumor cells and *in vivo* tumor models.

Materials and Methods

Test Compound

AG-012986, 4-[4-amino-5-(2,6-difluoro-benzoyl)-thiazol-2-ylamino]-*N*-(2-dimethylamino-1*R*-methyl-ethyl)-benzamide dihydrochloride was synthesized by the Pfizer Chemist (16). For *in vitro* assays, 10 mmol/L stock solutions of the compound were prepared in 100% DMSO. The routine vehicle of AG-012986 for *in vivo* administration was 30% polyethylene glycol 400 in aqueous 5% dextrose.

Kinase Assays

CDK activity was measured by monitoring the incorporation of [γ-^{32}P]ATP into a fragment of the Rb protein or histone H1 in 96-well plates using microfiltration and phosphoimaging as described previously (17). The K_i was measured by fitting the dose-dependent inhibition of CDKs to an equation for tight-binding competitive inhibition. Kinase counterscreening was conducted via in-house kinase assays, via commercial services, or in collaboration with the University of Dundee, and IC_{50}s were determined from four-variable fits of the dose-dependent inhibition of enzymes in the presence of ATP concentrations = K_m.

Cell Culture and Cell Assays

All cell lines used in our study, except MV522, were obtained as frozen stocks from American Type Culture Collection and cultured in RPMI 1640 supplemented with 10% FCS. Human MV522 tumor cells were provided by Dr. Michael Kelner (University of California-San Diego). For tumor cell proliferation studies, cells from log-phase growth cultures in 96-well plates were treated with various concentrations of AG-012986 at 37°C. After 72 h, cell viability was measured by the 3-(4,5-dimethylthiazol-2-yl)-2,5-2H-diphenyltetrazolium bromide assay. Tumor cell survival (colony-forming assay) was done by seeding 150 cells into 60-mm-diameter dishes for 4 h followed by treatment with AG-012986 at various concentrations for different periods before drug removal. Colonies were visible in 2 to 3 weeks for counting. IC_{50}s were calculated by using nonlinear four-variable curve fitting.

Cell Cycle Distribution

Cells in mid-log-phase growth were treated with AG-012986, and at termination, both detached and adherent cells were harvested. Cell cycle analysis was done with a FACSCalibur flow cytometry system (Becton Dickinson) using the CycleTEST Plus kit (Becton Dickinson).

Terminal Deoxynucleotide Transferase–Mediated dUTP Nick End Labeling Assay

Terminal deoxynucleotide transferase–mediated dUTP nick end labeling (TUNEL)/4,6-diamidino-2-phenylindole staining (the DeadEnd Colorimetric TUNEL System; Promega) was done to detect apoptosis using immunofluorescence microscopy. Slides were scored based on the percentage of positive FITC-stained cells (apoptotic) versus 4,6-diamidino-2-phenylindole–stained cell counts (total). The final score was obtained from the average count in five representative fields per slide.

Western Blots

Cell or tissue lysates were subjected to Western blot analysis as described previously (18). Primary antibody for phospho-Rb was rabbit anti-human phospho-Rb Ser^{795} (Cell Signaling; 1:300 dilution) and secondary antibody was conjugated goat anti-rabbit (Cell Signaling; 1:1,000 dilution). Poly(ADP-ribose) polymerase (PARP) cleavage was assessed by using rabbit anti-PARP IgG (Santa Cruz Biotechnology; 1:1,000 dilution). β-Actin protein expression was determined as an internal standard. The protein level of phospho-Rb Ser^{795} was quantified using the FluorChem 8800 digital image system (Alpha Innotech).

In vivo Studies

All animal husbandry and experimental procedures conducted complied with the Guide for the Care and Use of Laboratory Animals (ILAR, 1996) and were approved by the Pfizer Global Research and Development La Jolla Institutional Animal Care and Use Committee. The pharmacokinetics and antitumor efficacy of AG-012986 in mice were evaluated following i.p. injection in 5 mL/kg or s.c. infusion via implanted minipumps at 0.5 μL/h for a period of 7 days (Alzet).

Sample Analysis and Pharmacokinetic Calculations

Whole blood was collected retro-orbitally from three to five mice per treatment group for each time point. Plasma was prepared immediately and an internal standard was added in the plasma before protein precipitation with a mixture of acetonitrile and methanol (50:50, v/v). AG-012986 concentrations were analyzed using Quattro Ultima triple-quad mass spectrometry (Waters). Typically, 50 μL supernatant was injected onto a 50 × 2.1 mm/XDB-C18 column (Agilent) and the compound was eluted with a gradient of 35% to 93% acetonitrile in water over 3 min at a flow rate of 0.4 mL/min. Pharmacokinetic variables were calculated using the noncompartmental model of WinNonlin Professional Software version 4.0.1 (Pharsight).

In vivo Efficacy Evaluation and Sample Collection for Pharmacodynamic Analysis

Severe combined immunodeficient or athymic NCr-*nu/nu* mice were obtained from Charles River Breeding Laboratories. Tumor models were chosen based on *in vitro* response to CDK inhibitors, genetic status, and robustness. Two million cells were suspended in 30% (v/v) Matrigel (VWR) at a final volume of 200 μL and implanted in the dorsal region of mice. When tumor volumes reached 100 to 150 mm^3, mice were randomized and 10 to 12 mice were placed in each group. Treatments for efficacy studies were done using doses at or below the maximum tolerated dose. The maximum tolerated dose in mice, defined as the dose that induced <10% drug-related weight loss with no other adverse effect, was assessed before efficacy studies. Tumors were measured two to three times weekly using calipers and tumor volume was calculated as 0.5 × [length × width^2]. Additional details for each experiment are given in the table or figure legends.

Tumor samples for pharmacodynamic analysis were collected from mice in efficacy studies. BrdUrd pulse was done by i.p. administration of 30 mg/kg BrdUrd to tumor-bearing mice 2 h before tumor harvest. Excised tumor pieces were either fixed in 10% formalin for immunohistochemical analysis or snap frozen in liquid nitrogen for Western analysis.

Immunohistochemistry

Immunohistochemistry was done on paraffin-embedded tumor sections. The slide preparation and antigen retrieval were done as described previously (19, 20). For Ki-67 staining, rabbit monoclonal antibody (Lab Vision; 1:800 dilution) and goat anti-rabbit IgG (DAKO; 1:200 dilution) were used as primary and secondary antibodies, respectively. BrdUrd immunohistochemical staining was done with a biotin-conjugated monoclonal antibody (Zymed/Invitrogen; 1:20 dilution) followed by incubation with an avidin-biotin-peroxidase complex (Vectastain ABC kit, Vector Laboratory). Quantitative measurement of Ki-67- or BrdUrd-positive cells was determined using the Chromovision automated cell imaging system.

Statistical Analysis

Statistical analysis was conducted using Prism software (GraphPad). One-way ANOVA followed by Dunnet's *t* test was done to assess the significant difference between the tumor volumes of the vehicle and AG12986-treated groups when the mean tumor volume in the vehicle-treated group reached 700 to 800 mm^3.

Results

CDK Inhibition, Selectivity, and Broad-Spectrum Ligand-Binding Profile of AG-012986

As an ATP-competitive inhibitor, AG-012986 displays nanomolar potency (K_i) against the cell cycle CDKs, CDK4/cyclin (9.2 nmol/L), CDK2/cyclin A (94 nmol/L), and CDK1/cyclin B (44 nmol/L). CDK9/cyclin T and CDK5/p35 were also inhibited, with an IC_{50} of 4 and 22 nmol/L, respectively. The selectivity of AG-012986 against a diverse panel of kinases is shown in Table 1A. AG-012986 showed at least 100-fold selectivity for CDK4 over the kinases profiled, with the exception of calmodulin-dependent kinase II (~50-fold selective). AG-012986 was also profiled against 64 receptors, ion channels, and transporters in radioligand binding assays (Table 1B). Only three of these potential off-target interactions showed IC_{50}s of <10 μmol/L that translated into functional activity in subsequent cell- or tissue-based assays. AG-012986 displayed antagonism toward the calcium type L ion channel and the serotonin transporter with K_is of 2.44 and 2.26 μmol/L, respectively, and agonism for the histamine H3 receptor with a K_i of 0.837 μmol/L.

Cellular Activity of AG-012986

The antiproliferative activity of AG-012986 was tested against a panel of human tumor cell lines in culture (Table 2A). The average IC_{50} of AG-012986 against the 18 cell lines was 120 nmol/L (55 ng/mL). In 13 of 18 cell lines tested, AG-012986 displayed IC_{50}s of <100 nmol/L, showing its broad-spectrum antiproliferative activity. The antiproliferative activities of AG-012986 were independent of the genetic status of p53 and Rb.

In vitro Effects of AG-012986 on Rb Ser^{795} Hypophosphorylation, Cell Cycle, and Apoptosis

As one of the known natural substrates for CDKs, Rb would be expected to become hypophosphorylated upon drug-induced inhibition of CDKs (21–23). Of the 16 known phosphorylation sites on Rb, Ser^{795} can be phosphorylated by CDK2/cyclin A, CDK2/cyclin E, and CDK4/cyclin D1. Thus, a phosphospecific antibody to Ser^{795} of Rb was used to investigate the effect of AG-012986 on the phosphorylation status of Rb Ser^{795}. As determined by Western blot, treatment of asynchronous HCT116 human colon cancer cells with AG12986 resulted in a concentration-dependent loss of Rb phosphorylation at the Ser^{795} site. Treatment of HCT116 tumor cells with up to 240 nmol/L AG-012986 showed minimal effects on the status of phospho-Rb Ser^{795} at 8 h after treatment (Fig. 1A). However, after 24-h treatment, 60 to 240 nmol/L AG-012986 induced dose-dependent Rb Ser^{795} hypophosphorylation, with maximal effects at >120 nmol/L. These results indicate that treatment with AG-012986 for >8 h is required for achieving the hypophosphorylation.

The cell cycle response of AG-012986 on tumor cells was evaluated using flow cytometry (Fig. 1B). When HCT116 cells were treated with concentrations of AG-012986 between 30 and 120 nmol/L for 24 h, cell cycle distribution analysis exhibited accumulation of cells in G_1 phase of the cell cycle, consistent with CDK4 inhibition. However, when cells were treated with AG-012986 at ≥240 nmol/L, G_2-phase accumulation was observed after 24 h, consistent with CDK1 inhibition. Cell cycle analysis results also indicated that transient exposure (<8 h) of AG-012986 at concentrations up to 1 μmol/L failed to induce any sign of cell cycle arrest (data not shown). To further investigate the downstream effect of CDK inhibition by AG-012986 *in vitro*, we assessed apoptosis post-treatment by the TUNEL assay using immunofluorescence microscopy. HCT116 cells were

Table 1.

(A) Structure and kinase activity of AG-012986

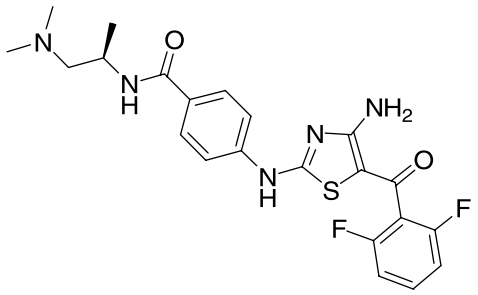

Enzyme*	K_i (nmol/L)
CDK4/cyclin D3	9.2
CDK2/cyclin A	94
CDK1/cyclin B	44
Enzyme†	%Inhibition at 1 μmol/L
CDK7/cyclin H	0
CDK3/cyclin E	46
CDK5/p35	IC_{50}, 22 nmol/L
CDK9/cyclin T‡	IC_{50}, 4 nmol/L
GSK3β	48
Calmodulin-dependent kinase II	54 (IC_{50}, 475 nmol/L)
ROCK-II	33
PRK-2	25
c-RAF, PRAK, CK-1, PKBα, AMPK,	<20

(B) Secondary pharmacology selectivity panel

Receptor, transporter, ion channel§	Binding K_i (μmol/L)	Functional result	Tissue source
Adenosine A_{2A}	0.47	None	Platelets (human)
Calcium channel type L	1.6, 2.4‖	Antagonist	Ileum (guinea pig)
Histamine H_3	0.837	Agonist	Ileum (guinea pig)
Serotonin transporter	2.26	Antagonist	Left atria (guinea pig)
Sodium channel site 2	5.9	None	HEK-293 (human)

*K_i of AG-012986 was >10,000 nmol/L against cyclic AMP–dependent PK, Chk1, JUNK, c-Src TK, VEGF RTK, P-FGF RTK, P-LCK TK, and P-IRK RTK. K_i of AG-012986 was >1,000 nmol/L against ERK2, PKC, and FAK.

†AG-012986 at 1 μmol/L showed 0% Inhibition against MEK-1, MKK6, SAPK2b, SAPK2a, MAPKAP-K2, MSK-1, SGK, P70S6K, ZAP-70, JNK3, MAPK-1, JNK2α2 and JNK1α1.

‡Test was done in Millipore.

§Tests were done at MDS Pharm Services. AG-012986 was screened against 64 receptors, transporters, and ion channels at 6.5 μmol/L. These included receptors from the adenosine, adrenergic, bradykinin, dopamine, endothelin, epidermal growth factor, estrogen, γ-aminobutyric acid, glucocorticoid, glutamate, histamine, imidazoline, interleukin, leukotriene, muscarinic, neuropeptide Y, nicotinic, opiate, phorbol ester, platelet-activating factor, purinergic, serotonin, sigma, tachykinin, and testosterone families as well as norepinephrine, dopamine, and serotonin transporters, and calcium, potassium, and sodium ion channels. Those showing >50% inhibition were assessed for inhibition constant (K_i) and for functional agonism or antagonism.

‖Values for displacement of benzothiazepine and dihydropyridine, respectively.

treated with AG-012986 at concentrations ranging from 30 to 240 nmol/L for 8 or 24 h. At 8 h, no apoptosis was observed (data not shown). At 24 h, AG-012986 at ≥120 nmol/L induced a greater proportion of apoptotic cells (Fig. 1C) than control conditions, with an IC_{50} of ~160 nmol/L (curve not shown). Apoptosis induced by AG-012986 (240 nmol/L) in HCT116 cells was confirmed by assessing PARP cleavage and electron microscopy (Supplementary Figs. S1 and S2).[6]

The colony-forming assay assessed tumor cell survival under varying treatment durations to assess net cell kill (Fig. 1D). SW620 human colon carcinoma cells were treated for different periods to assess tumor cell survival. At the desired time points (8, 24, 72, and 320 h), the treatment was stopped by removing medium containing AG-012986 before continuing growth in fresh medium. At time points ≥72 h, substantial cytotoxicity (IC_{50} <100 nmol/L) of AG-012986 was shown. Moderate activity with an IC_{50} of 300 nmol/L was observed at 24 h, whereas minimal cytotoxic activity was observed at the 8-h time point. These results suggest that a minimum of 24-h treatment duration is desired for AG-012986 to show efficacy. Similar results were observed in other cell lines.

Antitumor Efficacy in Various Human Xenograft Tumor Models

The *in vivo* efficacy of AG-012986 was evaluated at or under maximum tolerated dose (35-40 mg/kg/d; 8-12 days) in s.c. implanted human tumor xenograft models. The dosing period varied depending on the tumor growth rate and generally covered the tumor exponential growth period. The results of representative studies of different tumor models are summarized in Table 2B. AG-012986 showed >83% tumor growth inhibition (TGI) in 10 of the 11 tumor models tested. Figure 2 shows the dose-dependent efficacy of AG-012986 against COLO205 colon carcinoma (Fig. 2A) and NCI-H522 non-small cell lung carcinoma (Fig. 2B) when mice were treated at different doses daily for 12 days. In mice bearing COLO205 tumors, AG-012986

[6] Supplementary material for this article is available at Molecular Cancer Therapeutics Online (http://mct.aacrjournals.org/).

was able to induce net log tumor cell kill of 1.20 and 0.64 (Fig. 2C) when dosed at 40 and 20 mg/kg, respectively. In the NCI-H522 tumor model, AG-012986 dosed at 35 and 17.5 mg/kg produced 83.1% and 48% TGI, respectively, but without net log tumor cell kill (Fig. 2D).

Pharmacodynamic Endpoints Assessment

In parallel with the *in vivo* efficacy evaluations, tumors from satellite groups were harvested for pharmacodynamic analysis. COLO205 tumors were harvested at 8 and 24 h after mice received a single i.p. injection of efficacious (20 and 40 mg/kg) or nonefficacious (10 mg/kg) doses of AG-012986. Phospho-Rb Ser^{795} status and PARP cleavage in tumor extracts was assessed by Western blot (Fig. 3A). After 24 h, efficacious doses (20 and 40 mg/kg) of AG-012986 reduced Rb Ser^{795} phosphorylation by >80% relative to controls and induced concomitant PARP cleavage. A nonefficacious dose (10 mg/kg) of AG-012986 only reduced Rb Ser^{795} phosphorylation by 50% and failed to cause PARP cleavage. A decrease in phospho-Rb Ser^{795} and cleaved PARP (data not shown) was not observed at any dose at the 8-h time point. In addition to Rb Ser^{795} hypophosphorylation, time-dependent inhibition of cell cycle arrest was observed in COLO205 tumors following i.p. administration of AG-012986. S phase, as estimated by BrdUrd uptake in COLO205 tumors (Fig. 3B), significantly decreased between 12 and 24 h after mice were administered a single dose of AG-012986 (20 mg/kg). Dose-dependent Rb Ser^{795} hypophosphorylation was also shown in MV522 tumor-bearing

Table 2.

(A) Antiproliferation of AG-012986 against tumor cell lines in culture

Cell line	Origin	p53 status	Rb status	IC_{50} (μmol/L)*
COLO205	Colon carcinoma	Mutant	Wild-type	0.049
SW620	Colon carcinoma	Mutant	Wild-type	0.083
HCT116	Colon carcinoma	Wild-type	Wild-type	0.030
MV522	Lung carcinoma	Mutant	Wild-type	0.19
H522	Lung carcinoma	Mutant	Wild-type	0.26
H460	Lung carcinoma	Wild-type	Wild-type	0.50
MDA-MB-468	Breast carcinoma	Mutant	Mutant	0.27
MDA-MB-435	Breast carcinoma	Mutant	Wild-type	0.056
MDA-MB-453	Breast carcinoma	Mutant	Wild-type	0.045
ZR-75-1	Breast carcinoma	Wild-type	Wild-type	0.087
A2780	Ovarian tumor	Wild-type	Wild-type	0.035
BXPC3	Pancreatic	Mutant	Wild-type	0.055
SAOS-2	Osteosarcoma	Loss	Mutant	0.09
RL	Lymphoma	Mutant	Wild-type	0.034
SR	Lymphoma	Wild-type	Wild-type	0.030
CCRF-CEM	Leukemia	Mutant	Wild-type	0.068
Molt-4	Leukemia	Wild-type	Wild-type	0.220
HL60	Leukemia	Mutant	Low	0.048

(B) AG-12986 *in vivo* antitumor efficacy against different tumor models

Tumor model	Dose (mg/kg/d)	Regimen†	%TGI‡
COLO205 colon	40	Days 1-12	94.7§
HCT116 colon	35	Days 1-12	84.4§
SW620 colon	40	Days 1-12	84.0§
H522 NSCLC	35	Days 1-12	83.1§
MV522 lung	35	Days 1-8	94§
MDA-MB-435 mammary	40	Days 1-12	59§
SR lymphoma	40	Days 1-12	113.7§
RL lymphoma	40	Days 1-12	97.5§
A2780 ovarian	35	Days 1-8	91.1§
CCRF-CEM	40	Days 1-12	84.2§
HL60 leukemia	40	Days 1-12	108§

*Concentration of AG-012986 necessary to inhibit cell proliferation by 50%.

†Indicates the treatment period via i.p. administration. Treatment period based on the tumor growth rate to ensure the treatment period is within the exponential growth range.

‡%TGI was calculated as $100 \times (1 - \Delta T / \Delta C)$. ΔC (ΔT) was measured by subtracting the mean tumor volume in the vehicle (treated) group on the first day of treatment from the mean tumor volume on the evaluation day. Tumor size was evaluated when the mean in the vehicle-treated group reached 750 mm^3.

§$P < 0.05$ (versus vehicle-treated group in each study by one-way ANOVA analysis followed by Dunnet's t test).

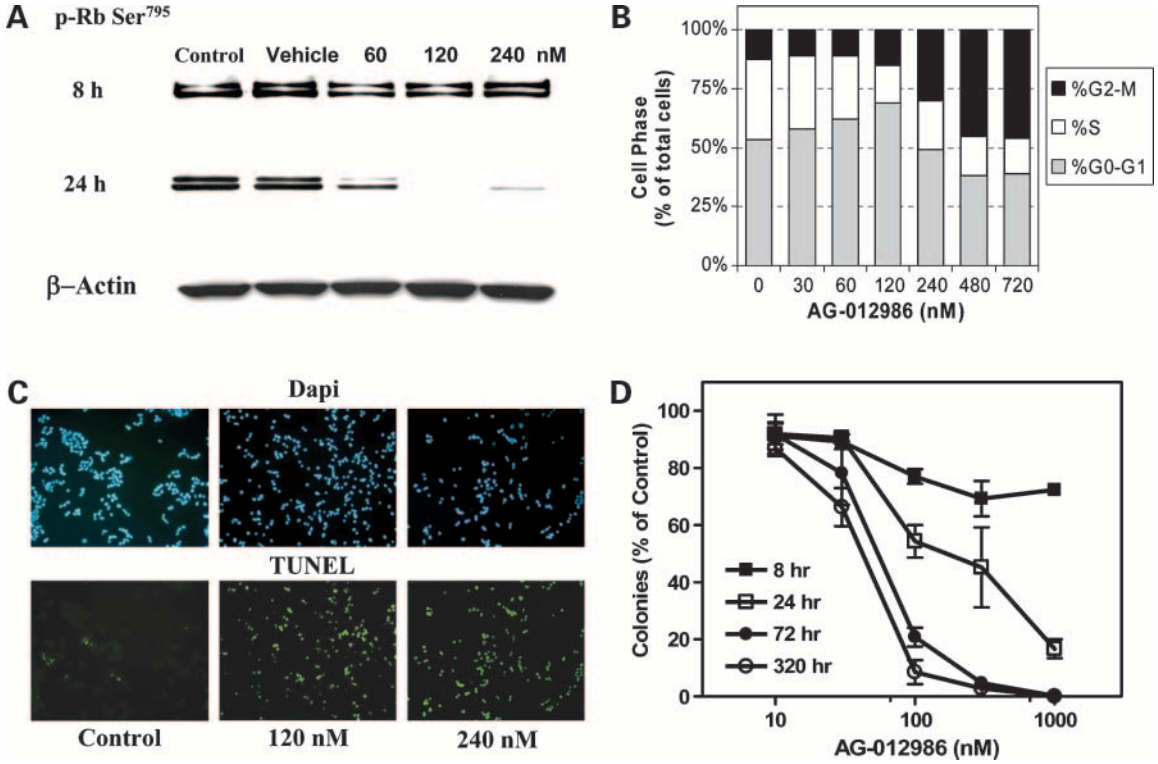

Figure 1. *In vitro* properties of AG-012986. **A,** AG-012986-induced inhibition of Rb phosphorylation in human tumor cells. Asynchronous HCT116 cells were treated with AG-012986 at the indicated concentrations for 8 and 24 h. Phospho-Rb status at the Ser^{795} site in cell extracts was assessed using an anti-phospho-Rb Ser^{795} antibody by Western blots. **B,** AG-012986-induced cell cycle arrest. HCT116 cells in mid-log phase were treated with various concentrations of AG-012986 for 24 h. Cells were then harvested and stained using the CycleTEST Plus kit (Becton Dickinson). Cell cycle analysis was done with a FACSCalibur flow cytometry system (Becton Dickinson). Cells undergoing apoptosis are gated out so only cells in the G_1, S, and G_2-M phases were included in the total population (100%) in each sample. **C,** AG-012986-induced apoptosis. HCT116 cells were treated with 120 and 240 nmol/L AG-012986 for 24 h before harvesting for TUNEL staining. 4,6-Diamidino-2-phenylindole and TUNEL staining represent the total number of cells and the number of cells going under apoptosis, respectively. **D,** a colony-forming assay showing time- and dose-dependent cell survival after AG-012986 treatment. Preseeded SW620 cells in 6-cm Petri dishes were treated with varying concentrations of AG-012986. At the indicated time, treatment was stopped by removing the medium containing AG-012986. Cells were washed with PBS before continuing growth in fresh medium until study termination. Data were normalized by designating the mean colony counts in vehicle treated samples as 100%. Mean ± SE of three points.

mice after a single administration of AG-012986. Moreover, there was a concurrent elimination of Ki-67-stained cells assayed by immunohistochemical staining. The decrease of phospho-Rb Ser^{795} and Ki-67 proliferation index in MV522 tumor correlates with the TGI (done in a separate study) induced by AG-012986 (Fig. 3C), suggestive of target-associated efficacy.

Pharmacokinetics and Dosing Schedule Optimization

The pharmacokinetic profile of AG-012986 in mice was evaluated following i.p. or s.c. implanted minipump administrations. These dosing regimens provided the opportunity to test the effects of plasma concentration or exposure profile on efficacy. In the tested dose range (12-75 mg/kg), AG-012986 via i.p. administration produced slightly greater than dose-proportional increases in C_{max} and AUC (Fig. 4A and C) with an average half-life of 1 h. In mice receiving AG-012986 via s.c. minipumps (Fig. 4B and D), the steady-state plasma levels were achieved within 6 to 24 h and remained relatively constant for up to 120 h post-implant. The daily $AUC_{0\text{-}24}$, estimated from average of the total $AUC_{0\text{-}168}$, was dose proportional in the range from 10 to 40 mg/kg/d. Mice receiving AG-012986 via a s.c. implanted pump displayed substantially (~30-fold) lower plasma levels in comparison with the C_{max} values achieved after i.p. bolus administration at similar doses.

Dosing optimization was done by comparing the efficacies of AG-012986 in COLO205 tumor-bearing mice using various dosing regimens via i.p. administrations or s.c. implanted pump infusion (Table 3). Due to dose proportionality, some AUC and C_{max} values in Table 3 were estimated based on the linear fit from the data in pharmacokinetic section (Fig. 4C). After a 7-day infusion at 20 mg/kg/d, mice in group 2 (Table 3) received a 3-day rest and the pump was replaced with a new pump infusing AG-012986 at the same dose. Significant efficacy (TGI, 77.1%) was observed in this group. Under a different dosing schedule, AG-012986 at 20 mg/kg/d via i.p. administration for 12 days (Table 3, group 1) induced 71.3% TGI. Although the total AUC and total dose were comparable between these two groups, the plasma C_{max} in group 2 (s.c. infusion pump) was significantly lower than that of group 1 dosed i.p. (0.273 versus 5.18 μg/mL). Higher

unsustained C_{max} values did not correlate with better efficacy. This relationship was further shown by comparing i.p. administration of AG-012986 at 40 mg/kg/d (group 4) with 20 mg/kg twice daily (group 5) for 8 days. The C_{max} value at 40 mg/kg was nearly twice as high as the C_{max} resulting from administration at 20 mg/kg twice daily; however, no proportional increase of efficacy was observed, suggesting that the efficacy of AG-012986 was not related to the C_{max}.

The effect of dosing interval on the efficacy of AG-012986 was also evaluated by comparing an intermittent dosing schedule with the schedule of daily administration. On a schedule of daily i.p. administration at 37.5 mg/kg, AG-012986 displayed 92.3% TGI (Table 3, group 7). Increasing the dosing interval from 24 to 48 h (group 8) resulted in less efficacy (TGI, 72.9%).

The effects of total dose or total exposure on efficacy of AG-012986 were evaluated by adjusting the ratio of daily dose to treatment period. AG-012986 administration at 40 mg/kg/d for 7 days (280 mg/kg total) via s.c. pump (Table 3, group 3) delivery displayed moderate efficacy (TGI, 47.9%). However, better efficacy (77.1%) was seen when the same total dose was delivered by expanding the dosing period to 2 weeks at a lower daily dose (20 mg/kg/d) via two sequentially implanted pumps (Table 3, group 2).

Discussion

AG-012986 showed the characteristics expected of a pan-CDK inhibitor: the mechanism of action and pharmacodynamic studies show a correlation between pan-CDK inhibition and inhibition of cell growth, cell cycle effects, and induction of apoptosis. The molecule displayed potent inhibition of several cell cycle CDK enzymes, as well as inhibition of Rb phosphorylation *in vitro* and *in vivo*, in both a time- and dose-dependent manner. The inhibition of Rb phosphorylation correlated with cell growth inhibition in cell cultures and implanted tumors. The arrest of cells at both G_1 and G_2 phases, as well as hypophosphorylation of Ser^{780}, Ser^{821} (data not shown), and Ser^{795}, show the pan-CDK inhibitory activity of AG-012986. The cell cycle arrest, shown by fluorescence-activated cell sorting analysis *in vitro* and BrdUrd uptake *in vivo*, was consistent with the decrease in the clinically relevant proliferation

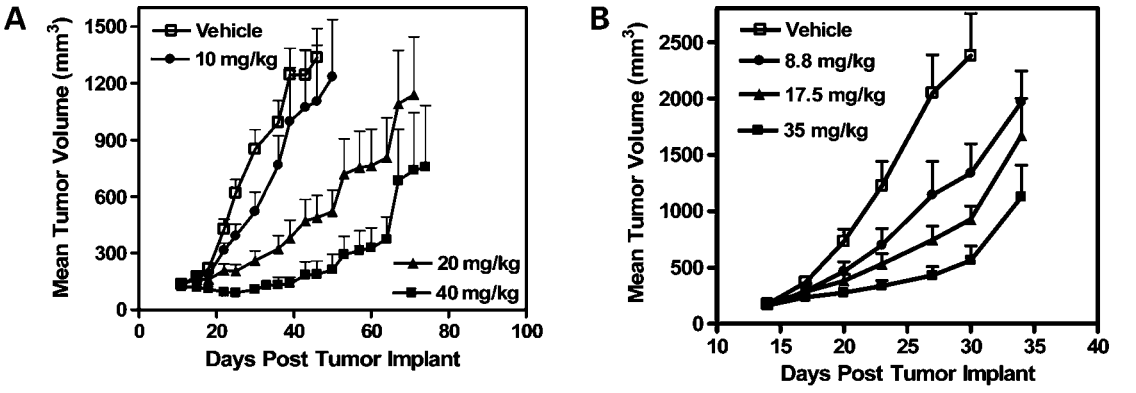

C

Dose (mg/kg)	TGI (%)	Growth Delay (Days)	Gross Log Kill	Net Log Kill
40	94.7 *	43	1.66	1.20
20	71.3 *	28.5	1.10	0.64
10	22.2	6.5	0.25	-0.21

D

Dose (mg/kg)	TGI (%)	Growth Delay (Days)	Gross Log Kill	Net Log Kill
35	83.1 *	12	1.03	0
17.5	48.0 *	8.5	0.73	-0.30
8.8	32.0	4	0.34	-0.69

Figure 2. Dose-dependent antitumor efficacy of AG-012986 against COLO205 (**A** and **C**) and H522 (**B** and **D**) xenograft models. Treatment commenced when median tumor volume in each group reached 100 to 150 mm^3. AG-012986 was i.p. administered once daily for 12 d at a volume of 5 mL/kg. Daily dosages are indicated in the graphs. Variables in **C** and **D**: %TGI was calculated as $100 \times (1 - \Delta T / \Delta C)$. ΔC (ΔT) was measured by subtracting the mean tumor volume in vehicle (treated) group on the first day of treatment from the mean tumor volume of the evaluation day, which is when the mean tumor size in vehicle-treated group reached 750 mm^3. Growth delay is the time difference (days) for the median treated tumor and control tumor to reach three doubling of the initial tumor size. Gross log kill was calculated as growth delay / ($3.32 \times$ tumor doubling time). Net log kill was calculated as (growth delay - treatment period) / ($3.32 \times$ tumor doubling time). The tumor doubling time, assessed from a log-linear growth plot of the control group tumors in exponential growth (100-800 mm^3) period, was estimated as 7.8 and 3.5 d for COLO205 and H522 tumor model, respectively. Net log tumor cell kill represents the change in tumor burden in response to therapy. A negative value indicates a net increase in tumor mass during therapy, whereas a positive value indicates tumor stasis after therapy. Values near 0 indicate tumor stasis during therapy. *, $P < 0.05$ by statistics test, which was done by comparing the tumor sizes between AG-012986-treated groups and vehicle-treated group using one-way ANOVA analysis followed by Dunnet's *t* test.

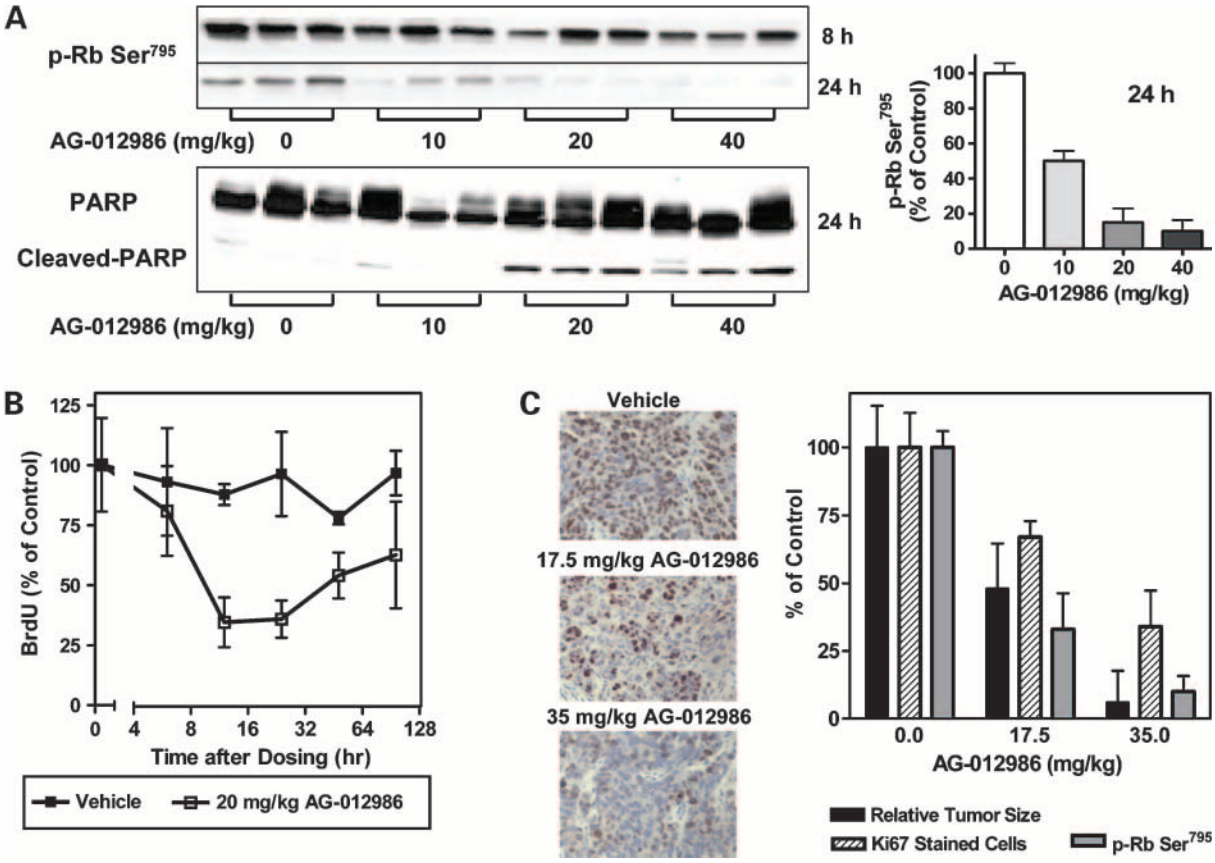

Figure 3. *In vivo* pharmacodynamic endpoints measurement after tumor-bearing mice were treated with AG-012986. **A,** AG-012986 induces time- and dose-dependent Rb Ser^{795} hypophosphorylation and PARP cleavage in COLO205 tumors. Mice bearing tumors in exponential growth period (300-400 mm^3) were i.p administered with a bolus dose of AG-012986. Tumors were harvested at 24 h after dosing. Rb Ser^{795} level in Western blots was quantitatively assessed using a digital image system (bar graph). **B,** BrdUrd uptake by COLO205 tumors after treatment with AG-012986. Tumor-bearing mice were dosed (i.p.) with 20 mg/kg AG-012986. Two hours before the tumor harvest, mice were administered (i.p.) with 30 mg/kg BrdUrd. Tumors were excised at the indicated time after the injection of AG-012986 and fixed for immunohistochemical analysis. BrdUrd staining was done according to the reagent manufacturer's instructions (Zymed). **C,** AG-012986 induces dose-dependent inhibition in tumor growth, decrease of Ki-67-positive cells, and Rb Ser^{795} hypophosphorylation in MV522 tumors. Tumor sizes were evaluated when mice (10 in each group) were i.p. administered with AG-012986 at the indicated dosage daily for 8 days. The evaluation day was when the mean tumor volume in vehicle-treated group reached 750 mm^3. For Ki-67 and phospho-Rb analysis, tumor-bearing mice were dosed (i.p.) with single injection of 17.5 and 35 mg/kg AG-012986. Three to five samples were collected and analyzed for each individual time point in the graph. At 24 h post-dose, tumors were collected for the assessment of phospho-Rb Ser^{795} status and Ki-67 proliferation index (IHC staining on the left). All data in Fig. 3 were normalized by designating the individual marker levels in vehicle-treated group as 100%.

biomarker, Ki-67. Another CDK inhibitor, PD0332991, has been shown to decrease Ki-67 in tumor sections (13), showing a common link between CDK inhibition and this biomarker.

The antiproliferative effects of CDK inhibitors could be attributed to a decrease in cell division or an increase in cell death (24). In HCT116 cells, immunofluorescent TUNEL staining showed apoptosis induced by AG-012986 with an IC_{50} of 160 nmol/L after 24 h of treatment (Fig. 1C). PARP cleavage and electron microscopy assessment (Supplementary Figs. S1 and S2)[6] further confirmed that AG-012986 (at 240 nmol/L) induced apoptosis. *In vivo*, apoptosis was also seen in COLO205 tumors via PARP cleavage after mice were treated with efficacious concentrations (20 and 40 mg/kg) of AG-012986 (24 h). The apoptosis induced by AG-012986 under both *in vitro* and *in vivo* settings occurred concomitantly with the hypophosphorylation of Rb Ser^{795} and cell cycle arrest, suggesting that the apoptosis was a downstream effect of cell cycle CDK inhibition. This finding agrees with literature reports that tumor cells treated with other cell cycle CDK inhibitors show an overall increase in apoptosis in a cell line–specific manner (25, 26). The fact that COLO205 tumors showed some net log cell kill after AG-012986 treatment for 12 days at 40 mg/kg shows the ability of the compound to induce tumor cell death *in vivo* with repeated dosing. Possible mechanisms of apoptosis could include deregulation of the feedback inhibition of CDK2/cyclin A, which could cause aberrant exit from S phase, or inhibition of CDK1-induced phosphorylation of the antiapoptotic proteins survivin or Mcl-1. Cell death could also arise from the depletion of the Mcl-1 antiapoptotic protein induced by CDK9 inhibition as was

reported for flavopiridol (12), seliciclib (7), and SU9516 (6) in hematopoietic tumor cells. However, the onset of apoptosis in those studies was significantly more rapid (3-5 h) than observed for AG-012986. At efficacious concentrations/doses, AG-012986 did not induce apoptosis within 8 h. The sum of these data suggests that the major mechanism of antitumor activity of AG-012986 is via inhibition of the cell cycle CDKs, although we cannot exclude the possibility that some cytotoxicity may be attributed to off-target effects.

The duration of treatment of tumor cells with a cell cycle CDK inhibitor would be expected to be critical. *In vitro*, tumor cells treated with AG-012986 at efficacious concentrations showed dose-dependent Rb Ser^{795} hypophosphorylation in 24 h but not 8 h (Fig. 1A). The colony-forming assay also emphasized the value of treatment duration on *in vitro* efficacy; minimal cytotoxic effects were observed following 8-h exposure of AG-012986, whereas better efficacy was observed when SW620 cells were treated for $\geq$24 h (IC_{50} <300 nmol/L). In order for AG-012986 to inflict target-associated cytotoxicity *in vivo*, maintenance of plasma levels at or above efficacious concentrations (C_{eff}) was required for extended periods. The exact efficacious concentration (C_{eff}) of AG-012986 in the mouse model was not defined in this report and was estimated from the *in vitro* antiproliferation assay (IC_{50} = 55 ng/mL, total). The unbound fraction of AG-012986 in mouse plasma is ~20%, whereas ~60% is unbound in the *in vitro* antiproliferation assay. Taking into account the differences in plasma protein binding, the estimated *in vivo* C_{eff} is ~165 ng/mL.

The pharmacokinetic and pharmacodynamic data suggest that maintaining plasma levels of the CDK inhibitor at or above C_{eff} over a dosing period is a better predictor of antitumor activity than acutely achieved C_{max}. The *in vivo* antitumor efficacy of AG-012986 was independent of C_{max}, as comparable efficacies were observed between groups administered 20 mg/kg via i.p. bolus daily for 12 days and s.c. implanted minipump for 14 days (Table 3). In addition, AG-012986 dosed (i.p.) at 40 mg/kg/d for 8 days produced similar efficacy (TGI, 45.8%) to 20 mg/kg twice daily (TGI, 47.1%); the higher C_{max} value did not yield increased efficacy. The *in vivo* efficacy evaluation results are consistent with the *in vitro* pharmacodynamic data showing that transient exposure (<8 h) of AG-012986 even at high concentrations (1,000 nmol/L) failed to induce Rb Ser^{795} hypophosphorylation and cell cycle arrest (data not shown). Further evidence of the correlation of efficacy with treatment duration rather than peak plasma levels was shown by comparing two groups of mice that were given the same total dose via s.c. implanted minipumps (Table 3,

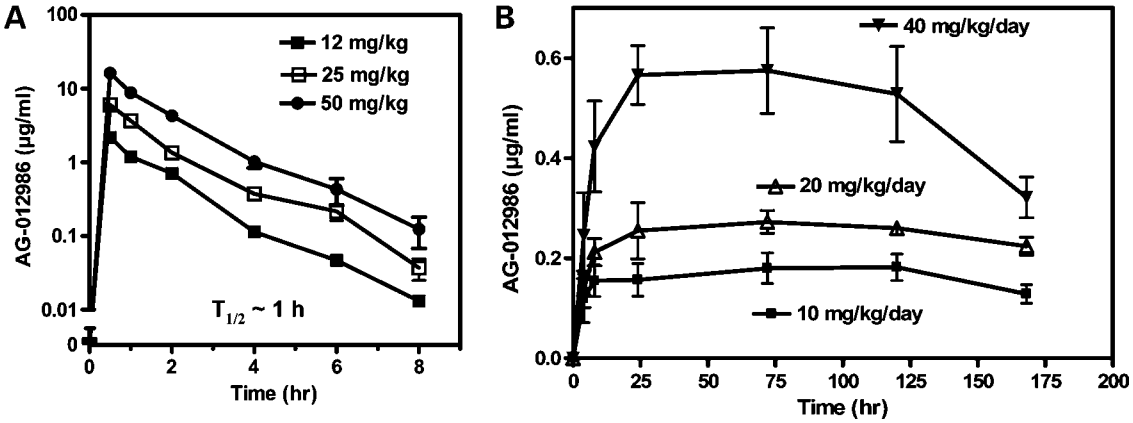

C

Dose (mg/kg)	C_{max} (µg/ml)	AUC (µg.h/ml)
6	1.08	1.32
12	2.17	3.32
25	6.02	8.74
50	16.23	23.62
75	22.50	44.66

D

Dose (mg/kg)	C_{max} (µg/ml)	AUC_{0-24} (µg.h/ml)	AUC_{0-168} (µg.h/ml)
10	0.182	3.92	27.5
20	0.273	5.97	41.8
40	0.575	12.00	84.0

Figure 4. AG-012986 pharmacokinetics. The plasma concentration versus time profile for AG-012986 is shown following i.p. bolus administration (**A**) and s.c. implantation of a minipump for 7-d infusion in mice (**B**). Pharmacokinetics variables of AG-012986 are tabulated representing values from a bolus i.p. administration (**C**) and s.c. implantation of a minipump for 7-d infusion (**D**). **A** and **B,** mean ± SE of three to five points. The dose given in each graph represents a daily administration of AG-012986 via s.c. pump or i.p. administration. **C** and **D,** AUC represents the area under the concentration between dosing. AUC_{0-168} represents the area under the concentration between 0 and 168 h (7 d) after dose (**D**). AUC_{0-24} values in **D** are calculated from AUC_{0-168}.

Table 3. Dosing optimization: relationship of pharmacokinetic variables and antitumor efficacies of AG-012986 against COLO205 tumor model

Group	Daily dose (mg/kg)	Each dose (mg/kg)	Route	Regimen*	C_{max} (μg/mL)†	AUC (μg h/mL)†	Total AUC (μg h/mL)‡	Total dose (g)‡	%TGI§
1	20	20	i.p.	Days 1-12	5.2	6.2	74.4	240	71.3‖
2	20	—	s.c. pump	Days 1-7, 11-18	0.273	6.0	83.6	280	77.1‖
3	40	—	s.c. pump	Days 1-7	0.575	12.0	84.0	280	47.9‖
4	40	40	i.p.	Days 1-8	12.3	17.3	138.7	320	45.8‖
5	40	20	i.p.	Days 1-8, b.i.d.	5.2	12.4	99.2	320	47.1‖
6	40	40	i.p.	Days 1-12	12.3	17.3	208.1	480	94.7‖
7	37.5	37.5	i.p.	Days 1-12	10.9	16.0	191.5	450	92.3‖
8	18.6	37.5	i.p.	Days 1-24, q.o.d.	10.9	8.0	191.5	450	72.9‖

Abbreviations: s.c. pump, s.c. implanted minipump; b.i.d., dosing twice daily; q.o.d., once every other day.
*Indicates treatment period. For i.p. route, single administration daily was done unless specified.
† C_{max} and daily exposure (AUC) via i.p. administration was estimated based on the linear fit from the data in Fig. 4C due to dose proportionality.
‡ Total AUC and total dose are the total values through out the whole study.
§%TGI was calculated as $100 \times (1 - \Delta T / \Delta C)$. ΔC (ΔT) was measured by subtracting the mean tumor volume in vehicle (treated) group on the first day of treatment from the mean tumor volume of the evaluation day. The evaluation day is when the mean tumor size in vehicle-treated group reached 750 mm^3.
‖ $P < 0.05$ (versus vehicle-treated group in each study by one-way ANOVA analysis followed by Dunnet's t test). The evaluation day is when the mean tumor size in vehicle-treated group reached 750 mm^3.

groups 2 and 3). AG-012986 displayed better efficacy (77.1%) at 20 mg/kg for 14 days compared with 40 mg/kg for 7 days (47.9%). Not surprisingly, these results suggest that, for the same total AUC, better efficacy is achieved if the plasma concentration is maintained at or above the C_{eff} (165 ng/mL) for extended periods. A similar relationship between pharmacokinetics and efficacy has been observed with other CDK inhibitors. For the initial clinical development of flavopiridol, a long continuous infusion schedule (24-72 h) was implemented based on preclinical studies demonstrating that longer period of drug exposure time improved the efficacy (27, 28). Seliciclib was also reported to have better target-associated efficacy as exposure time increased to 16 h (29).

Dosing optimization was further done by comparing between dosing intervals of 24 and 48 h for 12 i.p. injections of AG-012986 at 37.5 mg/kg. AG-012986 appeared less efficacious when the dosing interval was increased from 24 to 48 h (Table 3). An extended duration of subefficacious plasma concentrations of AG-012986 could allow tumor cells to escape cell cycle arrest and begin proliferating. Pharmacodynamic endpoint assessment indicated that the largest decrease of BrdUrd uptake occurred between 12 and 24 h after i.p. administration of AG-012986. After 24 h, tumor cells started to proliferate, as indicated by increasing BrdUrd uptake, again emphasizing the importance of extended maintenance of drug plasma levels above C_{eff} for extended duration for cell cycle inhibition.

The goal of dosing optimization is to maximize the therapeutic potential of a drug while minimizing the risks for toxicity. AG-012986 has been reported to show toxicities that are likely specific to this compound and are inconsistent with its expected pharmacologic mechanism. Acute peripheral leukocyte toxicity, retinal toxicity, and peripheral nerve toxicity (17, 30) were shown in toxicology studies in which mice were dosed i.v. with AG-012986. The C_{max} levels (>10 μmol/L) in those studies were higher than those achieved in the efficacy studies reported herein. Clearly, achieving a high plasma concentration (C_{max}) for a short duration (<8 h) is not desired for maximizing the therapeutic window of AG-012986, because it would not yield better efficacy but rather would cause potential safety issues. Therefore, dosing optimization of this type of cell cycle inhibitor is important not only to maximize efficacy by extending the duration of minimally efficacious plasma levels but also to minimize toxicities that are more likely to occur from high plasma levels.

The efficacies of flavopiridol (31, 32) and seliciclib (29), the most advanced CDK inhibitors under clinical development (33), were also reported to be dependent on dose and duration of exposure in solid tumors. Seliciclib displayed limited efficacy in phase I trials (10) possibly because the plasma concentrations could not be maintained at the micromolar concentrations for extended periods that are required for efficacy (>16 h; ref. 33). Flavopiridol has also displayed disappointing efficacy in the clinic, again possibly due to the challenges of maintaining sufficiently high free plasma concentrations of the drug (27, 28). These findings indicate that an ideal therapeutic CDK inhibitor should have sufficient potency and selectivity against the primary targets as well as a pharmacokinetic profile that enables *in vivo* cytoreductive activity with manageable safety risks. A newer generation of CDK inhibitors, PD0332991 (13) and R547 (34), are reported to have more desirable features, such as high oral bioavailability and longer plasma half-lives, as well as robust antitumor efficacies in preclinical studies. Although the question remains whether CDK inhibitors can be developed as single-agent therapeutics, some clinical investigators have recently focused on combination studies with CDK inhibitors, based on the hypothesis that CDK inhibitors can induce specific perturbations in the cell cycle and signal

transduction pathways that lower the threshold for cytotoxic agent-induced lethality against tumor cells without increasing safety risks (8, 9). For example, flavopiridol displayed sequence-dependent cytotoxic synergy with chemotherapy agents in clinical trials (9).

In summary, we have outlined the broad-spectrum antitumor activity of AG-012986 both *in vitro* and *in vivo*. The results from pharmacodynamic endpoint assessments in solid tumor lines are consistent with the antiproliferative mechanism expected for a pan-CDK inhibitor. A clear dose- and time-dependent connection between CDK inhibition, Rb hypophosphorylation, cell cycle arrest, suppression of tumor cell proliferation, and tumor cell apoptosis was established both *in vitro* and *in vivo* for AG-012986. In addition, dosing schedule optimization with AG-012986 showed that the plasma levels should be maintained at or above the C_{eff} (165 ng/mL) for >8 h daily to achieve antitumor activity and at least 72 h to maximize the potential for tumor cytotoxicity. Higher C_{max} plasma levels offer little or no added antitumor efficacy and may lead to dose-limiting toxicities; thus, a dosing regimen of the CDK inhibitor should be managed such that a minimal difference between C_{max} and C_{trough} levels is maintained throughout each treatment cycle. The lessons learned from AG-012986 may apply to pan-CDK inhibitors in general and help guide development of future CDK drug candidates.

Acknowledgments

We thank all of the Pfizer La Jolla CDK Project team members for the intellectual contribution to this work.

References

1. Kerkhoff E, Ziff EB. Cyclin D2 and Ha-Ras transformed rat embryo fibroblasts exhibit a novel deregulation of cell size control and early S phase arrest in low serum. EMBO J 1995;14:1892 – 903.

2. Kato JY, Matsuoka M, Polyak K, Massague J, Sherr CJ. Cyclic-AMP-induced G_1 phase arrest mediated by an inhibitor (p27Kip1) of cyclin-dependent kinase 4 activation. Cell 1994;79:487 – 96.

3. Kiess M, Gill RM, Hamel PA. Expression of the positive regulator of cell cycle progression, cyclin D3, is induced during differentiation of myoblasts into quiescent myotubes. Oncogene 1995;10:159 – 66.

4. Shan B, Farmer AA, Lee WH. The molecular basis of E2F-1/DP-1-induced S-phase entry and apoptosis. Cell Growth Differ 1996;7:689 – 97.

5. Wall NR, O'Connor DS, Plescia J, Pommier Y, Altieri DC. Suppression of survivin phosphorylation on Thr^{34} by flavopiridol enhances tumor cell apoptosis. Cancer Res 2003;63:230 – 5.

6. Gao N, Kramer L, Rahmani M, Dent P, Grant S. The three-substituted indolinone cyclin-dependent kinase 2 inhibitor 3-[1-(3H-Imidazol-4-yl)-meth-(*Z*)-ylidene]-5-methoxy-1,3-dihydro-indol-2-one (SU9516) kills human leukemia cells via down-regulation of Mcl-1 through a transcriptional mechanism. Mol Pharmacol 2006;70:645 – 55.

7. MacCallum DE, Melville J, Frame S, et al. Seliciclib (CYC202, *R*-roscovitine) induces cell death in multiple myeloma cells by inhibition of RNA polymerase II-dependent transcription and down-regulation of Mcl-1. Cancer Res 2005;65:5399 – 407.

8. Benson C, Kaye S, Workman P, Garrett M, Walton M, de Bono J. Clinical anticancer drug development. targeting the cyclin-dependent kinases. Br J Cancer 2005;92:7 – 12.

9. Shapiro GI. Preclinical and clinical development of the cyclin-dependent kinase inhibitor flavopiridol. Clin Cancer Res 2004;10:4270 – 5S.

10. Benson C, White J, De Bono J, et al. A phase I trial of the selective oral cyclin-dependent kinase inhibitor seliciclib (CYC202; *R*-roscovitine), administered twice daily for 7 days every 21 days. Br J Cancer 2007;96: 29 – 37.

11. Steven JM, Blake D, Clarke R, et al. *In vitro* and *in vivo* antitumor properties of the cyclin dependent kinase inhibitor CYC202 (*R*-roscovitine). Int J Cancer 2002;102:463 – 8.

12. Gojo I, Zhang B, Fenton RG. The cyclin-dependent kinase inhibitor flavopiridol induces apoptosis in multiple myeloma cells through transcriptional repression and down-regulation of Mcl-1. Clin Cancer Res 2002;8: 3527 – 38.

13. Fry DW, Harvey PJ, Keller PR, et al. Specific inhibition of cyclin-dependent kinase 4/6 by PD 0332991 and associated antitumor activity in human tumor xenografts. Mol Cancer Ther 2004;3:1427 – 38.

14. Tetsu O, McCormick F. Proliferation of cancer cells despite CDK2 inhibition. Cancer Cell 2003;3:233 – 45.

15. Ortega S, Prieto I, Odajima J, et al. Cyclin-dependent kinase 2 is essential for meiosis but not for mitotic cell division in mice. Nat Genet 2003;35:25 – 31.

16. Chong WKM, Chu S, Duvadie R, Xiao W, Yang Y, inventor; Agouron Pharmaceuticals, Inc., assignee. 4-Aminothiazole derivatives, their preparation, and their use as inhibitors of cyclin-dependent kinases. United States patent US 99/21845, 1998 Oct 27.

17. Jessen BA, Lee L, Koudriakova T, et al. Peripheral white blood cell toxicity induced by broad spectrum cyclin-dependent kinase inhibitors. J Appl Toxicol 2007;27:133 – 42.

18. Hinds PW, Mittnacht S, Dulic V, et al. Regulation of retinoblastoma protein functions by ectopic expression of human cyclins. Cell 1992;70: 993 – 1006.

19. Zou HY, Li Q, Lee JH, et al. An orally available small-molecule inhibitor of c-Met, PF-2341066, exhibits cytoreductive antitumor efficacy through antiproliferative and antiangiogenic mechanisms. Cancer Res 2007;67: 4408 – 17.

20. Gonchoroff NJ, Katzmann JA, Currie RM, et al. S-phase detection with an antibody to bromodeoxyuridine. Role of DNase pretreatment. J Immunol Methods 1986;93:97 – 101.

21. Lundberg AS, Weinberg RA. Functional inactivation of the retinoblastoma protein requires sequential modification by at least two distinct cyclin-cdk complexes. Mol Cell Biol 1998;18:753 – 61.

22. Beijersbergen RL, Carlee L, Kerkhoven RM, Bernards R. Regulation of the retinoblastoma protein-related p107 by G_1 cyclin complexes. Genes Dev 1995;9:1340 – 53.

23. Boulikas T. The phosphorylation connection to cancer [review]. Int J Oncol 1995;6:271 – 8.

24. Lane ME. A screen for modifiers of cyclin E function in *Drosophila melanogaster* identifies Cdk2 mutations, revealing the insignificance of putative phosphorylation sites in Cdk2. Genetics 2000;155:233 – 44.

25. Payton M, Chung G, Yakowec P, et al. Discovery and evaluation of dual CDK1 and CDK2 inhibitors. Cancer Res 2006;66:4299 – 308.

26. Ruetz S, Fabbro D, Zimmermann J, Meyer T, Gray N. Chemical and biological profile of dual Cdk1 and Cdk2 inhibitors. Curr Med Chem Anti-Canc Agents 2003;3:1 – 14.

27. Sedlacek HH. Mechanisms of action of flavopiridol. Crit Rev Oncol Hematol 2001;38:139 – 70.

28. Kaur G, Stetler-Stevenson M, Sebers S, et al. Growth inhibition with reversible cell cycle arrest of carcinoma cells by flavone L86-8275. J Natl Cancer Inst 1992;84:1736 – 40.

29. Raynaud FI, Whittaker SR, Fischer PM, et al. *In vitro* and *In vivo* pharmacokinetic-pharmacodynamic relationships for the trisubstituted aminopurine cyclin-dependent kinase inhibitors olomoucine, bohemine and CYC202. Clin Cancer Res 2005;11:4875 – 87.

30. Illanes O, Anderson S, Niesman M, Zwick L, Jessen BA. Retinal and peripheral nerve toxicity induced by the administration of a pan-cyclin dependent kinase (cdk) inhibitor in mice. Toxicol Pathol 2006;34:243 – 8.

31. Thomas JP, Tutsch KD, Cleary JF, et al. Phase I clinical and pharmacokinetic trial of the cyclin-dependent kinase inhibitor flavopiridol. Cancer Chemother Pharmacol 2002;50:465 – 72.

32. Zhai S, Senderowicz AM, Sausville EA, Figg WD. Flavopiridol, a novel cyclin-dependent kinase inhibitor, in clinical development. Ann Pharmacother 2002;36:905 – 11.

33. Fischer PM, Gianella-Borradori A. CDK inhibitors in clinical development for the treatment of cancer. Expert Opin Investig Drugs 2003;12:955 – 70.

34. DePinto W, Chu X-J, Yin X, et al. *In vitro* and *in vivo* activity of R547: a potent and selective cyclin-dependent kinase inhibitor currently in phase I clinical trials. Mol Cancer Ther 2006;5:2644 – 58.